AGU PUBLICATIONS

Geophysical Research Letters

RESEARCH LETTER
10.1002/2016GL072349

Key Points:
- Chlorophyll a concentrations are highly correlated with dry deposition flux ratios of soluble Fe/Cu
- The toxicity of aerosol Cu to phytoplankton could be alleviated by high Fe in the aerosol
- More frequent dust events may increase Fe/Cu flux ratio and contribute to the higher primary productivity in spring

Supporting Information:
- Text S1
- Figures S1–S5
- Tables S1–S4

Correspondence to:
Y. Chen,
yingchen@fudan.edu.cn

Citation:
Wang, F. J., Y. Chen, Z. G. Guo, H. W. Gao, K. R. Mackey, X. H. Yao, G. S. Zhuang, and A. Paytan (2017), Combined effects of iron and copper from atmospheric dry deposition on ocean productivity, *Geophys. Res. Lett.*, *44*, 2546–2555, doi:10.1002/2016GL072349.

Received 14 DEC 2016
Accepted 15 FEB 2017
Accepted article online 18 FEB 2017
Published online 4 MAR 2017

Combined effects of iron and copper from atmospheric dry deposition on ocean productivity

F. J. Wang[1], Y. Chen[1], Z. G. Guo[1], H. W. Gao[2], K. R. Mackey[3], X. H. Yao[2], G. S. Zhuang[1], and A. Paytan[4]

[1]Shanghai Key Laboratory of Atmospheric Particle Pollution Prevention, Department of Environmental Science and Engineering, Fudan University, Shanghai, China, [2]Key Lab of Marine Environmental Science and Ecology, Ministry of Education, Ocean University of China, Qingdao, China, [3]Earth System Science, University of California, Irvine, California, USA, [4]Institute of Marine Science, University of California, Santa Cruz, California, USA

Abstract Atmospheric deposition can provide nutrients and potential toxicants to marine ecosystem, hence affecting ocean net primary productivity (NPP). Nonetheless, the interactive effects of mixed aerosol components on phytoplankton have rarely been reported. Here we explored the combined effects of iron (Fe) and copper (Cu) on NPP over the East China Sea. In aerosol addition mesocosm experiments, phytoplankton growth was suppressed under high aerosol Cu but was increased when high Cu was accompanied by high Fe in aerosols. A time series of soluble aerosol Fe and Cu deposition was obtained and compared to regional chlorophyll *a* (Chl *a*) abundances from Moderate Resolution Imaging Spectroradiometer/Aqua. Strong positive correlations were observed between the dry flux ratios of soluble Fe/Cu and Chl *a* abundances in the large offshore area, whereas these variables were uncoupled in coastal regions where riverine input and upwelling dominated the biogeochemistry. Current work provides insight into the complex linkage between atmospheric deposition and marine productivity.

1. Introduction

Atmospheric aerosols supply nutrients and other substances to the ocean and may influence net primary productivity (NPP, supported by external source of nutrients such as atmospheric deposition) and carbon uptake [*Duce et al*., 2008; *Jickells et al*., 2005], hence affecting the atmospheric CO_2 and climate [*Mahowald*, 2011]. Recent studies show that the increase in nitrogen (N) availability in the western North Pacific is most likely due to deposition of atmospheric N pollutants, and this input may enhance primary production of the region [*Kim and Jeong*, 2011; *Kim et al*., 2014]. However, phytoplankton responses to atmospheric deposition can be complicated in areas with high loads of mixed natural and anthropogenic aerosols, such as the East China Sea (ECS).

The ECS is one of the most productive area of the world's ocean and currently a net sink of anthropogenic CO_2 [*Chen et al*., 2004]. The Changjiang river, the third longest in the world, discharges 9×10^{11} m^3/yr [*Liu et al*., 2007] water into the ECS and contributes a large amount of nutrients and carbon (as dissolved and particulate organic matter). Additional processes that affect the concentration of nutrients and trace elements in the ECS include transport from the Kuroshio Current [*Liu et al*., 2007], local upwelling, and atmospheric deposition [*Hsu et al*., 2009]. Human activities have increased the amount of atmospheric aerosols in the last few decades [*Rauch and Pacyna*, 2009]. Specifically, in East Asia, large quantities of aerosols are generated due to rapid industrialization, urbanization, and increases in traffic flow [*Parrish and Zhu*, 2009; *Kurokawa et al*., 2013]. In the offshore open water portion of the ECS, atmospheric deposition of terrigenous materials is the major source of trace elements to the surface ocean [*Hsu et al*., 2009; *Lin et al*., 2015].

Iron fertilization via dust transport and deposition stimulates phytoplankton growth in high nutrient low chlorophyll (HNLC) areas of the ocean [*Moore et al*., 2004; *Jickells et al*., 2005] and supports nitrogen fixation in oligotrophic seas because diazotrophs have high-Fe requirements [*Falkowski*, 1997]. Atmospheric Fe input has a strong impact on ocean productivity, with higher deposition values in the North Pacific, supporting >50% of the sinking biogenic Fe export in the Northern Hemisphere [*Krishnamurthy et al*., 2010]. Aerosols have also been suggested to support phytoplankton and bacterial activity in low-nutrient, low-chlorophyll regions of the ocean [*Moore et al*., 2004; *Chien et al*., 2016]. *Wang et al.* [2015a] investigated the influence

of atmospheric deposition (including N, phosphorus (P), and Fe) on primary productivity of the global ocean using the NEMO-PISCES model and found that anthropogenic N deposition from aerosols dominates the fertilizing effect on global ocean productivity. In their model Fe solubility is prescribed as an individual constant for each source and the available measurements for soluble Fe are about 3 orders of magnitude less than those of N and P, suggesting that large uncertainty may exist in the estimate of fertilization effect of aerosol Fe.

Aerosol deposition can also have toxic effects on marine phytoplankton, due to high concentrations of Cu or synergistic effects between various aerosol components [*Paytan et al*., 2009; *Jordi et al*., 2012]. It has been pointed out that the toxic effects of anthropogenic heavy metals such as Cu may disturb the stimulation of NPP by Fe [*Wang et al*., 2015a]. Accordingly, many on-deck incubation studies with dust addition showed rather different responses of chlorophyll *a* (Chl *a*) and productivity from those caused by direct addition of "pure" Fe(II) [*Coale et al*., 1996; *Meskhidze et al*., 2005]. Most previous studies [e.g., *Jordi et al*., 2012; *Kim et al*., 2014; *Moore et al*., 2004; *Paytan et al*., 2009] investigated the effect of individual aerosol component on ocean productivity, but the synergistic/antagonistic effects between two or more aerosol-derived elements have rarely been reported. Here we report results from mesocosm experiments and a comprehensive analysis on the relationships between dry deposition fluxes of soluble aerosol Fe and Cu and Moderate Resolution Imaging Spectroradiometer (MODIS)/Aqua Chl *a* concentrations in the ECS.

2. Materials and Methods

2.1. Aerosol Collection and Analysis

Aerosol samples were collected at Huaniao Island in the Zhoushan Archipelago (30.86°N, 122.67°E; Figure 1a), which is located in the northwestern ECS. This site was chosen because of its negligible local emissions and is thought to be representative of the regional aerosols transported to the ECS. Total suspended particulate (TSP) and size-segregated aerosol samples were collected using a high-volume sampler (1130 L min^{-1}; Thermo Scientific) and a nine-stage cascade impactor (28.3 L min^{-1}, Model FA-3, Anderson Company), respectively. The size-segregated samples are only used to obtain the size distribution of soluble Fe and Cu and estimate their dry deposition velocities [*Guo et al*., 2014]. Aerosols were collected on acid-cleaned Whatman® 41 cellulose filters. Collection times were 24 h for TSP and 72 h for the cascade impactor samples. Aerosol mass of each TSP sample was obtained by weighing the filter before and after aerosol collection. In total, 131 TSP and 22 size-segregated aerosol samples were collected during spring and winter of 2011 and the whole year of 2012. Sample numbers and blanks in each sampling period are listed in Table S1 in the supporting information.

One fourth cascade and 1/32 TSP samples were cut, respectively. The filter cuts and blank filters were extracted ultrasonically in 20 mL Milli-Q water (18.25 MΩ cm^{-1}) for 40 min. The extract was filtered immediately through a cellulose acetate membrane (pore size of 0.45 μm) and separated into two portions. One portion was analyzed for ions (oxalate) using ion chromatography (ICS3000, DIONEX). Another portion was acidified instantly with ultrapure HNO_3 (Guaranteed Reagent HNO_3 purified by a subboiling distillation) to the final concentration of 0.3 M. The concentrations of soluble elements were determined by Inductively Coupled Plasma Optical Emission Spectroscopy (SPECTRO, Germany). Detailed analytical procedures are provided in *Zhu et al.* [2013] and *Guo et al.* [2014]. The detection limits (DLs) for the soluble fractions of Fe and Cu in the size-segregated samples are both 0.01 nmol m^{-3}, and in the TSP samples DLs are 0.009 and 0.006 nmol m^{-3}, respectively. Organic carbon (OC) data for the same sampling periods are obtained from *Wang et al.* [2015b] by DRI Model 2001 thermal/optical Carbon Analyzer.

The soluble Fe and Cu concentrations determined using Milli-Q water in this study are expected to be higher than those dissolved in seawater. *Sholkovitz et al.* [2012] indicated that the fractional solubility of aerosol Fe is affected by various leaching solutions (pH 4.2–4.7 buffer solutions, pH 5.5 Milli-Q water and pH ~8 seawater) and leaching procedures (batch, flow through, and semicontinuous leaching methods). The Fe solubility could be ninefold higher in pure water than in seawater in a batch leaching [*Chen et al*., 2006], but such difference became insignificant when using flow through and semicontinuous leaching methods [*Buck et al*., 2010; *Aguilar-Islas et al*., 2010]. Although seawater leaches may provide the closest analog for the dissolution of dry aerosol in the surface ocean, pure water is a consistent and reproducible leaching solution facilitating comparison between studies, and also, its pH of 5.5 mimics the wet deposition [*Buck et al*., 2010].

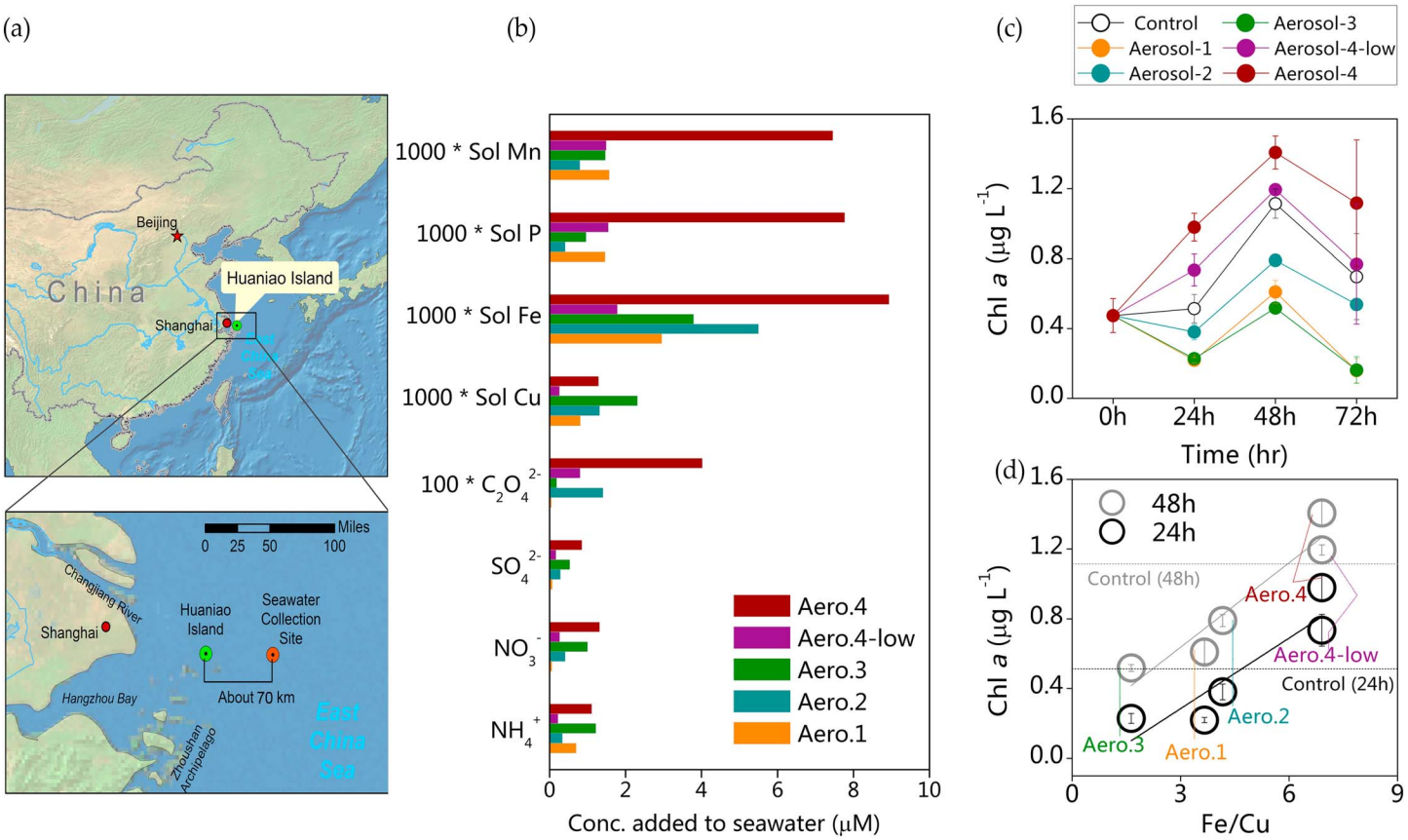

Figure 1. (a) Sites for the mesocosm experiment (Huaniao Island) and surface seawater collection (about 70 km east of Huaniao). (b) The concentrations of components added to seawater from the different aerosol samples. (c) The Chl *a* levels in different treatments of the mesocosm experiments at four selected time points (0 h, 24 h, 48 h, and 72 h). (d) The linear regressions between Chl *a* and soluble aerosol Fe/Cu (in molar ratios) added after 24 and 48 h incubation. Error bars represent one standard deviation.

2.2. Mesocosm Experiments

In situ mesocosm experiments were carried out at Huaniao Island (aerosol sampling site) using surface seawater (0–5 m) collected from a sampling site (30.85°N, 123.42°E) approximately 70 km east of the Island with the depth of the seafloor >50 m (Figure 1a). Although the salinity of the seawater was 29.9 ppt indicating the influence of Changjiang dilution water, the initial concentrations of NH_4^+, NO_3^-, and PO_4^{3-} (2.8, 2.5, and 0.12 μM, respectively) were low and the significant response of phytoplankton to the aerosol addition was expected.

Seawater samples were prefiltered with a 50 μm nylon mesh to remove zooplankton and stored in acid-cleaned 50 L white Tetrafluoroethylene (Nalgene®) carboys covered by double black plastic bags during transport to Huaniao Island (within 3 h). Approximately 2.2 L seawater was transferred into each 4 L polyethylene cubitainer, and aerosol filters were cut with 1 mg aerosols on each subsample and added to a final concentration of 0.45 mg L^{-1}. Four aerosol samples were chosen based on their chemical composition and corresponding backward trajectories determined from the NOAA Air Resource Lab Hybrid Single-Particle Lagrangian Integrated Trajectory (HYSPLIT) model [*Stein et al.*, 2015] (http://www.arl.noaa.gov/ready/hysplit4.html). These aerosols were characterized by high aluminum (indicating mineral dust; aerosol 1), high vanadium, and nickel (indicating ship emission; aerosol 2), relatively "clean day" condition with the lowest TSP of 61 μg m^{-3} (aerosol 3), and high-crustal tracer and secondary components (indicating combined dust and anthropogenic pollution; aerosol 4; Table S2). The addition amount was ~50% higher than the calculated dry flux estimated by assuming all deposition within a 10 m mixed layer depth over a 10 day period [*Park and Chu*, 2007]. The detailed calculation process and explanation are provided in the supporting information (Text S1). Aerosol 4 low represents 1/5 of the dose (0.09 mg L^{-1}) of aerosol 4 (Figure 1b).

The cubitainers were tied to a floating platform and submerged under surface seawater for 4 days. A neutral density shade was used to attenuate sunlight by 50% mimicking conditions in the upper 10 m of the euphotic zone. Temperature and salinity were measured using an YSI EC300 Multi-Parameter Water Quality Sonde (Yellow spring, OH). In order to minimize the risk of contamination, measurements were taken in triplicate for each treatment at four selected time points ($T_0 = 0$ h, $T_1 = 24$ h, $T_2 = 48$ h, and $T_3 = 72$ h). A volume of 350 mL seawater was filtered through GF/F filters under gentle vacuum filtration. Filters were frozen in cryovials at −20°C until processed. The protocol for Chl *a* analysis followed Method 445.0 (Elizabeth JA and Gray BC, 1997, EPA).

2.3. Dry Deposition Estimate

The dry deposition flux (F) of the soluble fraction of each aerosol element is estimated by multiplying its concentration in the TSP sample (C) by a size-dependent dry deposition velocity (V; Table S3). The V is determined individually for each element by multiplying the average mass percentage of the element for each stage of the size-segregated samples (R_i) by the deposition velocity calculated for the corresponding size bin (V_i) and then adding them together (equations (1) and (2)):

$$F = C \times V \tag{1}$$

$$V = \Sigma(R_i \times V_i) \tag{2}$$

In this study, we used Williams' model to predict particle deposition velocities for particles with aerodynamic diameters ranging between 0.05 and 100 μm, which covers the entire size range of particles collected by the nine-stage cascade impactor. The main formulas used in the model and a detailed derivation can be obtained from *Qi et al.* [2005].

2.4. Remote Sensing Analysis

The studied area of the ECS (26.9–32.9°N and 122.5–126.5°E) was divided into six zones with a size of 2° × 2° each for our remote sensing analysis (Figure 2a). The size was selected based on the satellite data spatial resolution and 50 m water depth line of the ECS. Smaller or larger areas will result in increased uncertainty of Chl *a* result due to less available data points and large Chl *a* variation range, respectively. In addition, using larger areas would hardly distinguish the coastal and open areas of ECS. Zones 1–3 (Z1, Z2, and Z3) are in the coastal area and have a water depth of less than 80 m while zones 4–6 (Z4, Z5, and Z6) are further offshore with depths greater than 100 m. The coastal water near the Changjiang estuary is highly turbid due to large amounts of suspended solids carried by riverine discharge and upwelling within the Zhoushan archipelago, which significantly affects zones Z1 and Z3 (Figure 2a). Relatively shallow depths (resuspension of sediments) and the Taiwan Warm Current show important impacts on zones Z2 and Z5, respectively (Figure 2b) [*Liu et al.*, 2007]. For Z4 and Z6, atmospheric deposition is the major external source of nutrients and trace elements to surface water [*Lin et al.*, 2015].

We use the satellite data of MODIS/Aqua Standard Level 3 Binned Chl *a* as an indicator of primary productivity as well as standard ,mapped image photosynthetically available radiation (PAR) and sea surface temperature (SST) (http://oceancolor.gsfc.nasa.gov). Data of Chl *a*, PAR and SST are extracted using SeaDAS 7.1 on a daily basis and at 4 km × 4 km (a pixel) for the period of March 2011 to January 2013. The Chl *a*, PAR and SST values of each zone are averaged across 2304 pixels (48 × 48 pixels) contained in the zone. We have eliminated Chl *a* concentrations greater than 20 mg m^{-3} (only one data point) and the dates with less than 10 valid data pixels, which may be associated with large uncertainties. Although an empirical algorithm has been used for estimating Chl *a* from the ocean color data for the ECS [*Ahn and Shanmugam*, 2006], MODIS/Aqua Chl *a* products are suggested to be better than those estimated by the local empirical algorithm [*Tan et al.*, 2011].

2.5. Automatic Linear Modeling

Automatic linear modeling in Statistical Product and Service Solutions (IBM® SPSS) was used to obtain a single model of the relationship between input predictor variables and response variables. It automatically transforms independent variables and uses outlier trimming and conducts model ensemble to improve predictions (all these features are not available in traditional regression analysis). It also provides both the stepwise and the all-possible subset methods (the latter is not available in regression) which are guided by multiple optimality statistics such as Akaike Information Criterion Corrected (AICC), adjusted R square, and overfit prevention criterion. (Regression has only significance test prone to Type I/II errors.) In this study,

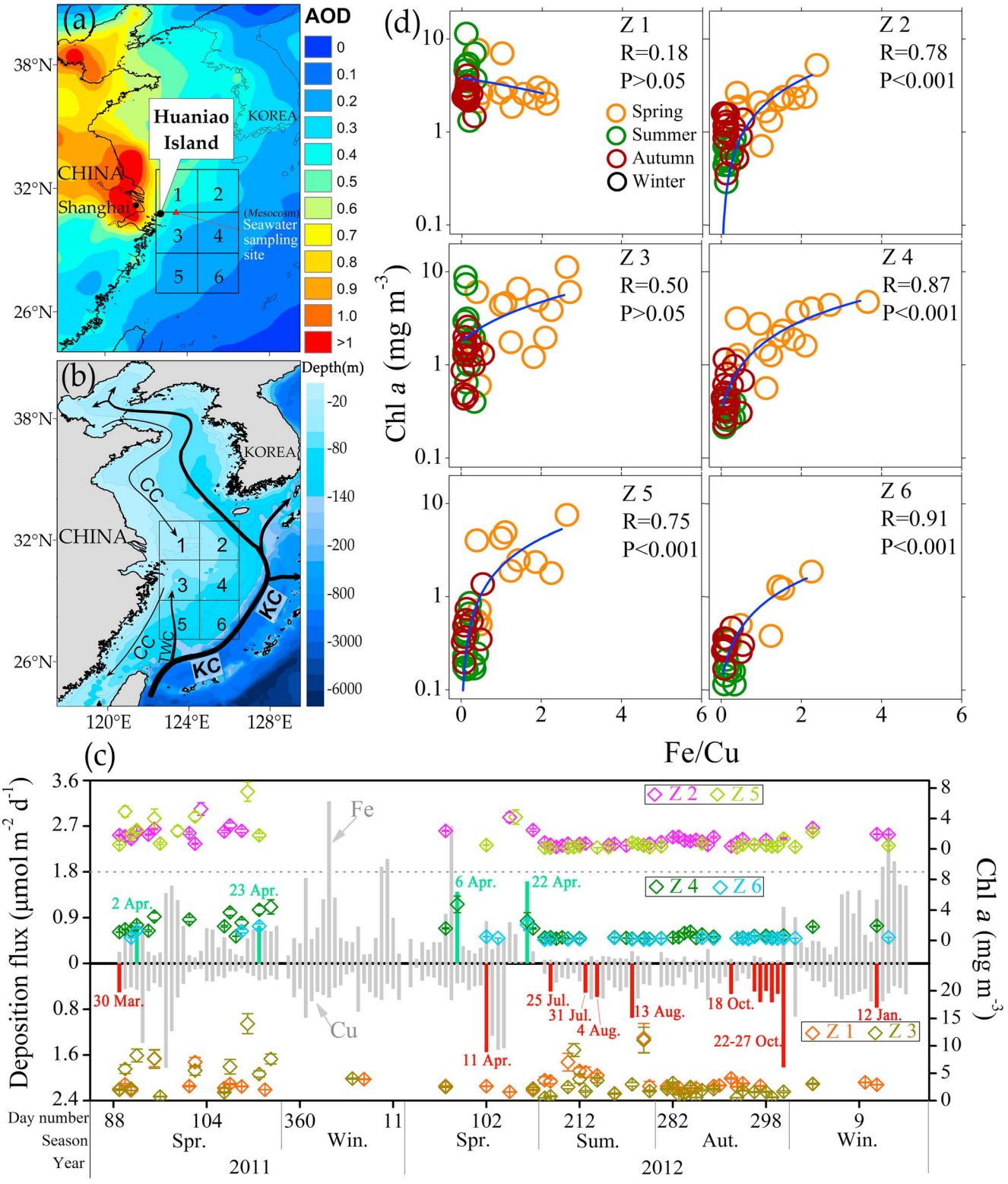

Figure 2. (a) The monthly averaged level of Aerosol Optical Depth (AOD) at 550 nm during our sampling period (from March 2011 to January 2013) over East Asia. (b) Bottom topography and the current system (black arrows) in the East China Sea. KC stands for the Kuroshio Current, CC stands for the Coastal Current, and TWC stands for the Taiwan Warm Current. (c) Dry deposition fluxes (left axis) of soluble Fe (gray bars; upward) and Cu (gray bars; downward) and the corresponding Chl *a* concentrations in the six zones (right axis) during the entire period. The colored columns indicate Fe and Cu deposition fluxes on specific dates, and the corresponding variations of Chl *a* are discussed in the text. Error bars represent 1 standard deviation. (d) The linear regression between Chl *a* (log10 scaling) and dry flux ratios of soluble Fe/Cu in each zone.

the Chl *a* concentration of each zone was a target and aerosol soluble components, including NH_4^+, NO_3^-, As, Cd, Co, Cr, Cu, Fe, Mn, P, Pb, V, Ni, and Zn, were predictors. During the Automatic Linear Modeling (ALM) operation the following options were selected: automatically prepare data, 95% confidence level, and forward stepwise model with maximum four steps. Criterion uses Akaike Information Criterion Corrected (AICC), which deals with the trade-off between the goodness of fit of the model and the complexity of the model.

3. Results and Discussion

3.1. Mesocosm Experiments

The ECS receives high fluxes of atmospheric aerosol deposition from natural and anthropogenic sources [*Hsu et al*., 2009; *Wang et al*., 2016]. To evaluate the effect of aerosols on marine phytoplankton over this region, we conducted mesocosm experiments by adding aerosols collected locally over Huaniao Island into ambient seawater. We found that Chl *a* concentrations increased significantly when adding aerosol 4 samples at both normal (simulating average deposition rates during high dust events) and low deposition (simulating deposition rates 1/5 lower than during dust events, aerosol 4 low). Addition of the other three aerosol samples resulted in a decrease in Chl *a* compared to control conditions (no addition) (Figure 1c). By comparing the amounts of aerosol components added, we found that aerosol 4 low had the lowest soluble Cu, NO_3^-, and NH_4^+ addition, but similar amounts of soluble Fe, P, and Mn compared to the aerosols 1, 2, and 3, respectively (Figure 1b). High concentration of aerosol Cu in the latter three treatments may inhibit phytoplankton growth, as has been demonstrated by previous studies [*Mann et al*., 2002; *Paytan et al*., 2009; *Jordi et al*., 2012]. Interestingly, aerosol 4 treatment contained similar amount of soluble Cu as the aerosols 1, 2, and 3 but showed a positive effect on growth, and we propose that the toxicity of aerosol Cu may be alleviated by relatively higher concentrations of soluble Fe, P, or Mn in aerosol 4 (Figure 1b). In fact, significant positive correlations ($R^2 = 0.9$) were found between Chl *a* concentrations and soluble aerosol Fe/Cu ratios in the mesocosm experiments (Figure 1d), and phytoplankton growth seemed to be constrained by both aerosol Fe (nutrient) and Cu (toxicant) and specifically their concentration ratio. Both soluble Fe (1.8–8.9 nM) and Cu (0.3–2.3 nM) concentrations derived from the aerosol additions (Figure 1b) were significant relative to the background levels of dissolved Fe (0.3–4.3 nM) and Cu (0.9–8.7 nM) in the ECS surface water [*Jiann et al*., 2009; *Jiann and Wen*, 2012; *Abe et al*., 2003], implying that the effects of aerosol Fe and Cu could be substantial in the experiments.

3.2. Significant Correlations Between Fe/Cu Flux Ratios and Chl *a*

Over the ECS, atmospheric input of dissolved Fe is ~10–100 times higher than that of the upwelling flux [*Hsu et al*., 2009]. Aerosols containing bioavailable Fe have been suggested to be an important factor (among others) that could trigger phytoplankton blooms in the oligotrophic South China Sea [*Wang et al*., 2012], and the high input of atmospheric Fe over the ECS may also play a significant role in controlling the primary productivity. In addition to Fe, which is derived primarily from mineral dust, the ECS is heavily affected by anthropogenic emissions from East Asia. Such aerosols are enriched with Cu, and the sharp increase in Cu deposition over the past decades may have altered primary productivity in this region [*Paytan et al*., 2009]. The concentrations of soluble aerosol Cu in our samples collected over Huaniao Island ranged from 0.08 to 2.03 nmol m^{-3} with an average of 0.53 nmol m^{-3}. This concentration is about sixfold higher than the low limit of aerosol Cu (~0.08 nmol m^{-3}) showing negative effect on phytoplankton growth over the western Mediterranean Sea [*Jordi et al*., 2012]. In short, the considerably high fluxes of Fe and Cu from the atmosphere to the ECS may affect the primary productivity, and synergy between Cu and Fe (or other constituents) may result in complex ecosystem responses.

To investigate the relationship between atmospheric input of Fe and Cu and NPP, we used the field measurements of daily aerosol composition over Huaniao Island during spring and winter of 2011 and the whole year of 2012, in conjunction with MODIS/Aqua standard level 3 binned Chl *a*, PAR and SST in the same periods [*Wang et al*., 2007]. The 8 day NPP data were also estimated from the Vertically Generalized Production Model (VGPM) at Ocean Productivity site [*Behrenfeld and Falkowski*, 1997]. A significant correlation was found between the NPP and Chl *a* with $R^2 = 0.68$ during 1 January 2011 to 31 December 2013 (Figure S1 in the supporting information). For each of six zones in this study, the significant correlations can also be seen between the NPP and Chl *a* as for the whole data set (Figure S1). The NPP calculation in the VGPM is

complex and is affected by many other factors such as physiological variability, day length, PAR, and euphotic depth. It is found that the photoacclimation-driven changes in chlorophyll have the opposite relationship to production as nutrient-driven/biomass-driven changes in Chl *a* [*Behrenfeld et al*., 2016]. Therefore, the record of surface Chl *a* may overrepresent associated changes in mixed layer productivity [*Behrenfeld et al*., 2016]. Even though Chl *a* concentration does not have a simple linear relationship with the NPP, Chl *a* and the rate of carbon fixation by phytoplankton both covary in response to environmental drivers [*Krishnamurthy et al*., 2010]. We note that the NPP data can be acquired only at relatively low resolution (8 day); thus, Chl *a* is used as an indicator of NPP in this study.

During the entire period, the average Chl *a* concentrations in the six zones in spring ranged between 1 and 4 mg m^{-3}; approximately onefold to threefold higher than those in winter (Figure 2c). The Chl *a* concentrations in winter are limited due to lack of MODIS/Aqua retrieval products. Peak Chl *a* concentrations that correspond to phytoplankton blooms occur under conditions of relatively high PAR (average 44 W m^{-2}) and SST (average 19°C) (Figure S2), which generally appear in spring for most zones with the exception of Z1 and Z3 (in both spring and summer). The relatively high fluxes of soluble aerosol Fe were also observed in spring (e.g., 2 and 23 April 2011 and 6 and 22 April 2012; Figure 2c, green bars) consistent with the East Asian winter monsoon and the most frequent Asian dust storm events. High-irradiance and increased Fe deposition in spring probably satisfied the light and Fe demand for phytoplankton growth [*Sunda and Huntsman*, 1997; *Moore et al*., 2006]. In contrast, the Chl *a* concentrations were found to be less than 1.2 mg m^{-3} on 25 July, 13 August, and 22–27 October 2012 for Z4 and Z6, when the soluble Cu fluxes were relatively high (Figure 2c, red bars). The rapid response (within 24 h) of phytoplankton to input of aerosol elements has been demonstrated in our mesocosm experiments (Figure 1d) and also by previous studies; rapid changes in Chl *a* concentrations have been observed in response to the change of trace elements, as well as diel cycles of photosynthesis and light intensity [*Singh et al*., 2008; *Pinedo-Gonzalez et al*., 2014]. We also note that the above relationships are not applicable in Z1 and Z3. High Chl *a* concentrations ($>$1.2 mg m^{-3}) are found to be associated with soluble Cu fluxes above average (0.38 μmol m^{-2} d^{-1}) in these two zones (e.g., 30 March 2011, 11 April, 31 July, and 4 August 2012; Figure 2c, red bars). This is probably due to the strong effect of Changjiang input and intense human activities in coastal area, which may have altered seawater chemistry (e.g., turbidity and organic ligands) and phytoplankton community structure [*Paytan et al*., 2009]. Extended periods of exposure to pollutant conditions could have allowed these coastal phytoplankton populations to adapt to high Cu levels [*Mackey et al*., 2012; *Meng et al*., 2016].

We focused our analysis of the correlations between Chl *a* and atmospheric input of substances in spring through fall because few Chl *a* retrievals are available in the winter, and relatively low PAR and SST can limit phytoplankton growth during this time. Significant positive relationships ($p < 0.05$) were found between Chl *a* and soluble aerosol Fe in the open ECS (Z2, Z4, Z5, and Z6) with correlation coefficients ranging between 0.4 and 0.7 (Figure S3). These results agree well with a recent study showing positive correlations ($r = 0.32$–0.57) between dust fluxes and Chl *a* concentrations in depths $>$50 m in the China Seas, but no correlation between the two variables in shallower $<$50 m China Seas [*Tan et al*., 2013]. Sufficient Fe supply carried by dust events may be the reason for observed algal blooms in the ECS [*Tan et al*., 2011]; Fe can stimulate the phytoplankton growth by accelerating photosynthesis, respiration, and nutrient uptake within cells [*Shaked et al*., 2005]. Besides Fe, other aerosol components may also show significant effects on ocean productivity.

Copper has been recognized as a primary toxicant in marine systems at elevated doses. Our mesocosm experiment demonstrates that high aerosol Cu may decrease Chl *a* concentration in ECS water. Automatic linear modeling shows that soluble aerosol Fe (positive effect) and Cu (negative effect) are the most important predictors of Chl *a* concentrations ($p < 0.001$) (e.g., in Z4; Figure S4). Notably, Chl *a* concentrations are highly correlated with the ratios of soluble aerosol Fe/Cu in Z2, Z4, and Z5 and Z6 ($R > 0.75$; $P < 0.001$; Figure 2d). The lack of significant relationships among these parameters in Z1 and Z3 are probably due to the strong influence of riverine discharge, shallow depth, and upwelling on the input of nutrients and trace elements in these zones. Besides, remote sensing standard Chl *a* product does not properly work for coastal areas with high turbidity, such as Z1 and Z3.

3.3. Mechanism of Coupled Constraint by Fe and Cu

Although organics in aerosols may detoxify Cu, the combined effect of Fe and Cu may be influenced more by the uptake and metabolism mechanisms of these two metals by the phytoplankton community than by

organic complexation. Soluble Fe concentrations in aerosols are found to be positively correlated with oxalate and organic carbon, suggesting that high amounts of organics may deposit along with high fluxes of soluble Fe (Figure S5). Copper toxicity alleviation by soluble aerosol Fe may be caused by the complexation of Cu by a relatively high content of organic ligands, which would largely decrease the concentration of free Cu^{2+}. Similarly, Fe bioavailability and the associated positive effects may also be impaired by this organic complexation. High irradiance in springtime not only enhances photosynthesis but also potentially enables the transfer of Fe (III) to soluble Fe (II) by direct photolysis of Fe(III) chelates or by reaction with photochemically produced superoxide radicals (O_2^-), thus facilitating Fe consumption by growing phytoplankton cells [*Maldonado and Price*, 2001; *Zepp*, 2003; *Pinedo-Gonzalez et al*., 2014]. Although Cu exhibits high affinity for low molecular weight organic matter, light can help move Cu from the colloidal pool (complexing with organic ligands) to the soluble pool via photolysis of colloidal organic matter or photoreduction of Cu (II) [*Pinedo-Gonzalez et al*., 2014]. Thus, organics in aerosols may not work effectively when aerosol Fe and Cu deposit into the surface seawater.

The combined effect of Fe and Cu on Chl *a* concentration is likely to vary in other oceanic regions with different phytoplankton community structure. Marine phytoplankton have developed physiological mechanisms to regulate Fe acquisition and utilization which depend on Cu [*Peers et al*., 2005; *Maldonado et al*., 2006]. Some eukaryotic microorganisms possess a Cu-dependent Fe transport system with Cu-containing ferroxidase, and they accumulate high amounts of Cu as Fe availability decreases [*Peers and Price*, 2006; *Annett et al*., 2008]. Indeed, Cu uptake by coastal diatoms was found to be minimized under Fe sufficient conditions [*Shaked et al*., 2005]. The uptake mechanism of bioavailable Fe is different between prokaryotes and eukaryotes [*Boyd and Ellwood*, 2010]. Alleviation of Cu toxicity by Fe may depend on which phytoplankton groups are present in seawater and may in turn result in changes of community structure. Diatoms are usually more tolerant than dinoflagellates to high Cu concentrations [*Quigg et al*., 2006; *Levy et al*., 2007], and the toxicity threshold for larger eukaryotic cell can be orders of magnitude higher than that of cyanobacteria [*Brand et al*., 1986]. Even within cyanobacteria different taxa show different resistance to Cu toxicity [*Paytan et al*., 2009], which has been proposed to shape the phytoplankton community structure in Sargasso Sea, particularly during the summer-stratified period [*Mann et al*., 2002]. It was also reported that high light-adapted ecotypes of *Prochlorococcus* are more resistant to Cu toxicity than its low light-adapted ecotype, which lives below the mixed layer [*Mann et al*., 2002].

4. Conclusion

Atmospheric input is one of the most important mechanisms for Fe input to the ocean and in HNLC areas this may enhance ocean productivity, while high loading of aerosol Cu resulting from human activities shows significant toxicity to the phytoplankton. Iron is required in the biosynthesis of Chl *a* and in the photosynthetic reactions and electron transport. The Fe-containing photosynthetic components include photosystem I and II, the cyt flb_6 complex, cytochrome c_6, and ferredoxin [*Raven et al*., 1999]. Iron is also a cofactor in a number of enzymes: catalase, peroxidase, chelatase, nitrogenase, and nitrate/nitrite reductases [*Sunda*, 2012, and references therein]. In contrast, high concentrations of Cu may induce proteomic changes [*Zou et al*., 2015], reduce cell division rates [*Brand et al*., 1986], and decrease photosynthetic rates [*Matilde et al*., 1995], all of which ultimately limit cell growth [*Guo et al*., 2012]. Our study demonstrates that under the conditions of appropriate PAR and SST, primary productivity in the large area of the ECS is constrained by soluble aerosol Fe/Cu dry deposition ratios. In fact, phytoplankton growth may respond to various components (e.g., NO_3^- and Ni could be important factors controlling NPP) from the atmospheric deposition in different regions of the ECS and within different periods; the complicated water masses and chemistry should be considered in the further study of the relationship between atmospheric deposition and ocean productivity. Higher Chl *a* concentrations in spring are likely associated with elevated Fe/Cu deposition ratios due to more frequent Asian dust storm events [*Hsu et al*., 2009] (Figure 2d). This demonstrates the crucial impact of dust transport and deposition on this marine ecosystem. Characterizing the interactive effects of aerosol Fe and Cu is an important step toward understanding the linkages between aerosol deposition and ocean productivity. The ECS is representative of marginal seas which are adjacent to the continents and influenced substantially by natural and anthropogenic emissions, and the coupled constraint of atmospheric deposition of Fe and Cu on primary productivity may be applicable in other similar ocean basins.

Acknowledgments

This work is jointly supported by the National Key Basic Research Program of China (2014CB953701), National Key Research and Development Program of China (2016YFA0601304), and National Natural Science Foundation of China (41375141). The data used are listed in the tables in the supporting information (curated by Fujiang Wang; jone_worf@126.com). The authors gratefully acknowledge the NOAA Air Resources Laboratory (ARL) for the provision of the HYSPLIT transport and dispersion model and/or READY website (http://www.ready.noaa.gov) used in this publication. We also thank the Ocean Biology Processing Group of NASA GSFC for ocean color data (acquired from http://oceancolor.gsfc.nasa.gov). We are grateful to Huaniao lighthouse maintained by Shanghai Maritime Safety Administration for providing the long-term sampling and experimental site.

References

Abe, K., Y. Ishihi, and Y. Watanabe (2003), Dissolved copper in the Yellow Sea and the East China Sea—Cu as a tracer of the Changjiang discharge, *Deep Sea Res., Part II*, *50*, 327–337.

Aguilar-Islas, A. M., J. Wu, and R. Rember (2010), Dissolution of aerosol-derived iron in seawater: Leach solution chemistry, aerosol type, and colloidal iron fraction, *Mar. Chem.*, *120*, 25–33.

Ahn, Y., and P. Shanmugam (2006), Detecting the red tide algal blooms from satellite ocean color observations in optically complex northeast-Asia coastal waters, *Remote Sens. Environ.*, *103*, 419–437.

Annett, A. L., S. Lapi, T. J. Ruth, and M. T. Maldonado (2008), The effects of Cu and Fe availability on the growth and Cu : C ratios of marine diatoms, *Limnol. Oceanogr.*, *53*, 2451–2461.

Behrenfeld, M. J., and P. G. Falkowski (1997), Photosynthetic rates derived from satellite-based chlorophyll concentration, *Limnol. Oceanogr.*, *42*, 1–20.

Behrenfeld, M. J., R. T. O'Malley, E. S. Boss, T. K. Westberry, J. R. Graff, K. H. Halsey, A. J. Milligan, D. A. Siegel, and M. B. Brown (2016), Revaluating ocean warming impacts on global phytoplankton, *Nat. Clim. Chang.*, *6*, 323–330, doi:10.1038/nclimate2838.

Boyd, P. W., and M. J. Ellwood (2010), The biogeochemical cycle of iron in the ocean, *Nat. Geosci.*, *3*, 675–682, doi:10.1038/ngeo964.

Brand, L. E., W. G. Sunda, and R. R. L. Guillard (1986), Reduction of marine phytoplankton reproduction rates by copper and cadmium, *J. Exp. Mar. Bio. Ecol.*, *96*, 225–250, doi:10.1016/0022-0981(86)90205-4.

Buck, C. S., W. M. Landing, J. A. Resing, and C. I. Measures (2010), The solubility and deposition of aerosol Fe and other trace elements in the North Atlantic Ocean: Observations from A16N CLIVAR/CO2 repeat hydrography section, *Mar. Chem.*, *120*, 57–70, doi:10.1016/j.marchem.2008.08.003.

Chen, C. T. A., A. Andreev, K. R. Kim, and M. Yamamoto (2004), Roles of continental shelves and marginal seas in the biogeochemical cycles of the North Pacific Ocean, *J. Oceanogr.*, *60*, 17–44, doi:10.1023/B:JOCE.0000038316.56018.d4.

Chen, Y., J. Street, and A. Paytan (2006), Comparison between purewater- and seawater-soluble nutrient concentrations of aerosols from the Gulf of Aqaba, *Mar. Chem.*, *101*, 141–152.

Chien, C.-T., K. R. Mackey, S. Dutkiewicz, N. M. Mahowald, J. M. Prospero, and A. Paytan (2016), Effects of African dust deposition on phytoplankton in the western tropical Atlantic Ocean off Barbados, *Global Biogeochem. Cycles*, *30*, 716–734, doi:10.1002/2015GB005334.

Coale, K. H., et al. (1996), A massive phytoplankton bloom induced by an ecosystem-scale iron fertilization experiment in the equatorial Pacific Ocean, *Nature*, *383*, 495–501, doi:10.1038/383495a0.

Duce, R. A., et al. (2008), Impacts of atmospheric anthropogenic nitrogen on the open ocean, *Science*, *320*, 893–897, doi:10.1126/science.1150369.

Falkowski, P. G. (1997), Evolution of the nitrogen cycle and its influence on the biological sequestration of CO_2 in the ocean, *Nature*, *387*, 272–275, doi:10.1038/387272a0.

Guo, J., S. Lapi, T. J. Ruth, and M. T. Maldonado (2012), The effects of iron and copper availability on the copper stoichiometry of marine phytoplankton, *J. Phycol.*, *48*, 312–325, doi:10.1111/j.1529-8817.2012.01133x.

Guo, L., Y. Chen, F. Wang, X. Meng, Z. Xu, and G. Zhuang (2014), Effects of Asian dust on the atmospheric input of trace elements to the East China Sea, *Mar. Chem.*, *163*, 19–27, doi:10.1016/jmarchem.2014.04.003.

Hsu, S.-C., S. C. Liu, R. Arimoto, T.-H. Liu, Y.-T. Huang, F. Tsai, F.-J. Lin, and S.-J. Kao (2009), Dust deposition to the East China Sea and its biogeochemical implications, *J. Geophys. Res.*, *114*, D15304, doi:10.1029/2008JD011223.

Jiann, K. T., and L. S. Wen (2012), Distribution and lability of dissolved iron in surface waters of marginal seas in southeastern Asia, *Estuar. Coast. Shelf Sci.*, *100*, 142–149.

Jiann, K. T., L. S. Wen, and G. C. Gong (2009), Distribution and behaviors of Cd, Cu, and Ni in the East China Sea surface water off the Changjiang estuary, *Terr. Atmos. Ocean. Sci.*, *20*, 433–443.

Jickells, T. D., et al. (2005), Global iron connections between desert dust, ocean biogeochemistry, and climate, *Science*, *308*, 67–71, doi:10.1126/science.1105959.

Jordi, A., G. Basterretxea, A. Tovar-Sanchez, A. Alastuey, and X. Querol (2012), Copper aerosols inhibit phytoplankton growth in the Mediterranean Sea, *Proc. Natl. Acad. Sci. U.S.A.*, *109*, 21,246–21,249, doi:10.1073/pnas.1207567110.

Kim, I. N., K. Lee, N. Gruber, D. M. Karl, J. L. Bullister, S. Yang, and T. W. Kim (2014), Chemical oceanography: Increasing anthropogenic nitrogen in the North Pacific Ocean, *Science*, *346*, 1102–1106, doi:10.1126/science.1258396.

Kim, T. W., and H. J. Jeong (2011), Increasing N abundance in the northwestern Pacific Ocean due to atmospheric nitrogen deposition, *Science*, *334*, 505–509, doi:10.1126/science.1206583.

Krishnamurthy, A., J. K. Moore, N. Mahowald, C. Luo, and C. S. Zender (2010), Impacts of atmospheric nutrient inputs on marine biogeochemistry, *J. Geophys. Res.*, *115*, G01006, doi:10.1029/2009JG001115.

Kurokawa, J., T. Ohara, T. Morikawa, and S. Hanayama (2013), Emissions of air pollutants and greenhouse gases over Asian regions during 2000–2008: Regional Emission inventory in ASia (REAS) version 2, *Atmos. Chem. Phys.*, *13*, 10,049–10,123, doi:10.5194/acpd-13-10049-2013.

Levy, J. L., J. L. Stauber, and D. F. Jolley (2007), Sensitivity of marine microalgae to copper: The effect of biotic factors on copper adsorption and toxicity, *Sci. Total Environ.*, *387*, 141–154, doi:10.1016/j.scitotenv.2007.07.016.

Lin, Y. C., J. P. Chen, T. Y. Ho, and I. C. Tsai (2015), Atmospheric iron deposition in the northwestern Pacific Ocean and its adjacent marginal seas: The importance of coal burning, *Global Biogeochem. Cycles*, *29*, 138–159, doi:10.1002/2013GB004795.

Liu, J. P., K. H. Xu, A. C. Li, J. D. Milliman, D. M. Velozzi, S. B. Xiao, and Z. S. Yang (2007), Flux and fate of Yangtze River sediment delivered to the East China Sea, *Geomorphology*, *85*, 208–224, doi:10.1016/j.geomorph.2006.03.023.

Mackey, K. R. M., K. N. Buck, J. R. Casey, A. Cid, M. W. Lomas, Y. Sohrin, and A. Paytan (2012), Phytoplankton responses to atmospheric metal deposition in the coastal and open-ocean Sargasso Sea, *Front. Microbiol.*, *3*, 359, doi:10.3389/fmicb.2012.00359.

Mahowald, N. (2011), Aerosol indirect effect on biogeochemical cycles and climate, *Science*, *334*, 794–796, doi:10.1126/science.1207374.

Maldonado, M. T., and N. M. Price (2001), Reduction and transport of organically bound iron by Thalassiosira oceanica (Bacillariophyceae), *J. Phycol.*, *37*, 298–310, doi:10.1046/j.1529-8817.2001.037002298.x.

Maldonado, M. T., A. E. Allen, J. S. Chong, K. Lin, D. Leus, N. Karpenko, and S. L. Harris (2006), Copper-dependent iron transport in coastal and oceanic diatoms, *Limnol. Oceanogr.*, *51*, 1729–1743.

Mann, E. L., N. Ahlgren, J. W. Moffett, and S. W. Chisholm (2002), Copper toxicity and cyanobacteria ecology in the Sargasso Sea, *Limnol. Oceanogr.*, *47*, 976–988.

Matilde, B., J. B. Arellano, and G. J. López (1995), Copper and photosystem II: A controversial relationship, *Physiol. Plant.*, *94*, 174–180.

Meng, X., Y. Chen, B. Wang, Q. W. Ma, and F. J. Wang (2016), Responses of phytoplankton community to the input of different aerosols in the East China Sea, *Geophys. Res. Lett.*, *43*, 7081–7088, doi:10.1002/2016GL069068.

Meskhidze, N., W. L. Chameides, and A. Nenes (2005), Dust and pollution: A recipe for enhanced ocean fertilization?, *J. Geophys. Res.*, *110*, D03301, doi:10.1029/2004JD005082.

Moore, C. M., M. M. Mills, A. Milne, R. Langlois, E. P. Achterberg, K. Lochte, R. J. Geider, and J. La Roche (2006), Iron limits primary productivity during spring bloom development in the central North Atlantic, *Global Change Biol.*, *12*, 626–634, doi:10.1111/j.1365-2486.2006.01122.x.

Moore, J. K., S. C. Doney, and K. Lindsay (2004), Upper ocean ecosystem dynamics and iron cycling in a global three-dimensional model, *Global Biogeochem. Cycles*, *18*, GB4028, doi:10.1029/2004GB002220.

Park, S., and P. C. Chu (2007), Synoptic distributions of thermal surface mixed layer and thermocline in the southern Yellow and East China Seas, *J. Oceanogr.*, *63*, 1021–1028.

Parrish, D. D., and T. Zhu (2009), Climate change: Clean air for megacities, *Science*, *326*, 674–675, doi:10.1126/science.1176064.

Paytan, A., K. R. Mackey, Y. Chen, I. D. Lima, S. C. Doney, N. Mahowald, R. Labiosa, and A. F. Post (2009), Toxicity of atmospheric aerosols on marine phytoplankton, *Proc. Natl. Acad. Sci. U.S.A.*, *106*, 4601–4605, doi:10.1073/pnas.0811486106.

Peers, G., and N. M. Price (2006), Copper-containing plastocyanin used for electron transport by an oceanic diatom, *Nature*, *441*, 341–344.

Peers, G., S. A. Quesnel, and N. M. Price (2005), Copper requirements for iron acquisition and growth of coastal and oceanic diatoms, *Limnol. Oceanogr.*, *50*, 1149–1158.

Pinedo-Gonzalez, P., A. J. West, I. Rivera-Duarte, and S. A. Sanudo-Wilhelmy (2014), Diel changes in trace metal concentration and distribution in coastal waters: Catalina Island as a study case, *Environ. Sci. Technol.*, *48*, 7730–7737, doi:10.1021/es5019515.

Qi, J. H., P. L. Li, X. G. Li, L. J. Feng, and M. P. Zhang (2005), Estimation of dry deposition fluxes of particulate species to the water surface in the Qingdao area, using a model and surrogate surfaces, *Atmos. Environ.*, *39*, 2081–2088, doi:10.1016/j.atmosenv.2004.12.017.

Quigg, A., J. R. Reinfelder, and N. S. Fisher (2006), Copper uptake kinetics in diverse marine phytoplankton, *Limnol. Oceanogr.*, *51*, 893–899, doi:10.4319/lo.2006.51.2.0893.

Rauch, J. N., and J. M. Pacyna (2009), Earth's global Ag, Al, Cr, Cu, Fe, Ni, Pb, and Zn cycles, *Global Biogeochem. Cycles*, *23*, GB2001, doi:10.1029/2008GB003376.

Raven, J. A., M. C. W. Evans, and R. E. Korb (1999), The role of tracemetals in photosynthetic electron transport in O_2-evolving organisms, *Photosyn. Res.*, *60*, 111–149.

Shaked, Y., A. B. Kustka, and F. M. M. Morel (2005), A general kinetic model for iron acquisition by eukaryotic phytoplankton, *Limnol. Oceanogr.*, *50*, 872–882, doi:10.4319/lo.2005.50.3.0872.

Sholkovitz, E. R., P. N. Sedwick, T. M. Church, A. R. Baker, and C. F. Powell (2012), Fractional solubility of aerosol iron: Synthesis of a global-scale data set, *Geochim. Cosmochim. Acta*, *89*, 173–189.

Singh, R. P., A. K. Prasad, V. K. Kayetha, and M. Kafatos (2008), Enhancement of oceanic parameters associated with dust storms using satellite data, *J. Geophys. Res.*, *113*, C11008, doi:10.1029/2008JC004815.

Stein, A. F., R. R. Draxler, G. D. Rolph, B. J. B. Stunder, M. D. Cohen, and F. Ngan (2015), NOAA's HYSPLIT atmospheric transport and dispersion modeling system, *Bull. Am. Meteorol. Soc.*, *96*, 2059–2077, doi:10.1175/BAMS-D-14-00110.

Sunda, W. G. (2012), Feedback interactions between trace metal nutrients and phytoplankton in the ocean, *Front. Microbiol.*, *3*, 1–22, doi:10.3389/fmicb.2012.00204.

Sunda, W. G., and S. A. Huntsman (1997), Interrelated influence of iron, light and cell size on marine phytoplankton growth, *Nature*, *390*, 389–392, doi:10.1038/37093.

Tan, S. C., G. Y. Shi, J. H. Shi, H. W. Gao, and X. H. Yao (2011), Correlation of Asian dust with chlorophyll and primary productivity in the coastal seas of China during the period from 1998 to 2008, *J. Geophys. Res.*, *116*, G02029, doi:10.1029/2010JG001456.

Tan, S.-C., X. Yao, H.-W. Gao, G.-Y. Shi, and X. Yue (2013), Variability in the correlation between Asian dust storms and chlorophyll *a* concentration from the north to equatorial Pacific, *PLoS One*, *8*, e57656, doi:10.1371/journal.pone.0057656.

Wang, F., Z. Guo, T. Lin, L. Hu, Y. Chen, and Y. Zhu (2015a), Characterization of carbonaceous aerosols over the East China Sea: The impact of the East Asian continental outflow, *Atmos. Environ.*, *110*, 163–173, doi:10.1016/j.atmosenv.2015.03.059.

Wang, F., Y. Chen, X. Meng, J. Fu, and B. Wang (2016), The contribution of anthropogenic sources to the aerosols over East China Sea, *Atmos. Environ.*, *127*, 22–33.

Wang, M. H., J. W. Tang, and W. Shi (2007), MODIS-derived ocean color products along the China east coastal region, *Geophys. Res. Lett.*, *34*, L06611, doi:10.1029/2006GL028599.

Wang, R., Y. Balkanski, L. Bopp, O. Aumont, O. Boucher, P. Ciais, M. Gehlen, J. Peñuelas, C. Ethé, and D. Hauglustaine (2015b), Influence of anthropogenic aerosol deposition on the relationship between oceanic productivity and warming, *Geophys. Res. Lett.*, *42*, 10,745–10,754, doi:10.1002/2015GL066753.

Wang, S. H., N. C. Hsu, S. C. Tsay, N. H. Lin, A. M. Sayer, S. J. Huang, and W. K. M. Lau (2012), Can Asian dust trigger phytoplankton blooms in the oligotrophic northern South China Sea?, *Geophys. Res. Lett.*, *39*, L05811, doi:10.1029/2011GL050415.

Zepp, R. G. (2003), *Solar UVR and Aquatic Carbon, Nitrogen, Sulfur and Metals Cycles: UV Effects in Aquatic Organisms and Ecosystems*, pp. 137–184, R. Soc. Chem., Cambridge, U. K.

Zhu, L., Y. Chen, L. Guo, and F. Wang (2013), Estimate of dry deposition fluxes of nutrients over the East China Sea: The implication of aerosol ammonium to non-sea-salt sulfate ratio in nutrient deposition of coastal oceans, *Atmos. Environ.*, *69*, 131–138.

Zou, H. X., Q. Y. Pang, A. Q. Zhang, L. D. Lin, N. Li, and X. F. Yan (2015), Excess copper induced proteomic changes in the marine brown algae Sargassum fusiforme, *Ecotox. Environ. Safe.*, *111*, 271–280, doi:10.1016/j.ecoenv.2014.10.028.